Applied Surface Science 643 (2024) 158681

Contents lists available at ScienceDirect

Applied Surface Science

journal homepage: www.elsevier.com/locate/apsusc

Full Length Article

Microstructural evolution and properties of He-charged a-Si coatings prepared by magnetron sputtering

V. Godinho [a,*], J. Caballero-Hernández [a], B. Lacroix [a,1], F.J. Ferrer [b,c], D. Jamon [d], M.C. Jiménez de Haro [a], A. Fernández [a,*]

[a] Instituto de Ciencia de Materiales de Sevilla CSIC- Uni. Sevilla, Av. Américo Vespucio 49, 41092 Sevilla, Spain
[b] Centro Nacional de Aceleradores, Universidad de Sevilla – CSIC- Junta de Andalucía, Av. Thomas A. Edison 7, 41092 Sevilla, Spain
[c] Departamento de FAMN, U. Sevilla, Aptdo 1065, 41012 Sevilla, Spain
[d] Université de Lyon, CNRS UMR 5516, Laboratoire Hubert Curien, Université Jean Monnet,18, Rue de Benoit Lauras, 4200 Saint Etienne, France

ARTICLE INFO

Keywords:
Helium bubbles
Porous silicon
Amorphous silicon
Band gap
Optical properties
Annealing effects

ABSTRACT

The introduction of porosity in nanomaterials via magnetron sputtering in helium atmospheres is an interesting strategy for the design of functional materials. Amorphous silicon coatings, with high concentration of He incorporated in the form of overpressurized nano-bubbles, present modified optical properties in comparison with dense coatings of similar composition.

In this work, annealing process in He atmosphere from 300 °C up to 1200 °C is performed to evaluate stability after the release of He from the a-Si:He coatings (thickness ~1700 nm) and to favor matrix crystallization and defect evolution. The work is focused on these effects on the silicon film and its properties. The composition and microstructural evolution of the coatings annealed to temperatures as high as 1200° were investigated by electron microscopy and X-Ray diffraction. Annealing effects on the optical properties and bandgap of the silicon coatings were evaluated by ellipsometry and UV–Vis spectrometry. Helium release from the coating, densification, defects evolution and ordering due to crystallization have a small effect on the refractive index, but cause a significant change in the material band gap from 1.37 eV to 1.80 eV.

1. Introduction

Over the last decades there has been an increasing interest on the nanostructuring of thin films and surfaces by low energy helium (He) plasma treatments [1–3], ion implantation [4] or by magnetron sputtering of thin films [5–11]. The very low solubility of He in different materials forming nanopores, can lead to bubbles containing high He density [7,12–14], voids [15] or to fine fuzz nanostructures[1,8]. The different obtained nanostructures have been paid attention, as a strategy for the design of functional materials, finding applications in photonic devices [16], solid He targets [12,17,18], solar light absorbers [19], photoactive materials for solar water splitting [20], anodes in rechargeable lithium batteries [9] or for decomposition of organic materials [21,22] among others. The formation of overpressurized He nano-bubbles [23] and its microstructural evolution [24] is a common feature to these approaches, which plays an essential role on the nanostructuration of these materials.

Among the different strategies, the formation of helium nanobubbles by ion implantation, either in metals or semiconductors, has been widely investigated. Several mechanisms have been proposed by different authors [13,25–27] to explain its nucleation and growth; mainly due to its implications in the nuclear physics community [11,27,28]. There is a common consensus that He atoms tend to aggregate and interact with host material defects, either by occupying available positions or by generating them when sufficiently high energy or ion dose is involved leading to extended defects as platelets or bubbles [13,29]. These defects in crystalline silicon have been promoted for example in semiconductor research on device applications as impurity getters [25,30], or for strain relaxation and smart cut in the SOI (Silicon-on-insulator) technology [31–33]. Similar formation of He bubbles was also reported for implanted amorphous silicon (a-Si) layers[33].

In our previous works we have proposed an alternative methodology to prepare a-Si layers with tailored refractive index by magnetron sputtering stabilizing high density of over pressurized He bubbles

* Corresponding authors.
E-mail addresses: godinho@icmse.csic.es (V. Godinho), asuncion@icmse.csic.es (A. Fernández).
[1] Current address: Escuela Politécnica Superior- Universidad de Sevilla, Departamento de Física Aplicada I, Calle Virgen de África 7, 41011 Sevilla, Spain.

https://doi.org/10.1016/j.apsusc.2023.158681
Received 13 June 2023; Received in revised form 3 October 2023; Accepted 14 October 2023
Available online 15 October 2023

[5,7,12]. Using pure helium, or mixtures of helium and argon [6] as deposition gas, coatings with huge He/Si content up to 0.79 [12] can be tailor-made, presenting He bubbles with sizes varying from 3 to 60 nm [5,7,12], that proved to be very stable in time (at least up to two years) and under low energy, low Z ion radiation [12]. Magnetron sputtering technique presents great advantages over implantation as it provides reproducible coatings, with homogeneous porosity and He concentration through the whole coating in a wide range of controlled thicknesses and on a broad variety of substrates, including polymers and porous membranes [5,16,34]. Moreover, the methodology is also suitable for the preparation of porous metallic or composite layers [10,23,34] on a laboratory scale, without the need for ion implantation facilities and that could be easily scaled up to an industrial process. Other authors have also investigated the incorporation of He into metallic films by magnetron sputtering in He/Ar atmospheres [3,11,27,35,36].

The introduction of defects by implantation and the formation of voids upon heat treatment, in crystalline silicon, are reported to induce deep levels in the silicon band gap [25,37] associated to the dandling bonds present on the internal nanobubble's surface[25]. It is described that during annealing treatments of implanted silicon at temperatures higher than 300 °C, helium permeates from bubbles leaving the crystalline matrix resulting in the formation of empty voids [4,25,38]. This mechanism of void formation can be of technological interest to selectively modify the recombination lifetime in silicon devices [39]. In the case of amorphous silicon films, the inherent disorder of the amorphous structure and the presence of dandling bonds have strong effect on the electronic density of states[40]. Helium nano-bubbles in a-Si film will increase the degree of structural disorder and dandling bonds. The aim of the present work is to investigate the annealing response of amorphous silicon coatings (thickness ~1700 nm) containing overpressurized He bubbles prepared by magnetron sputtering. Temperatures up to 1200 °C were used for a complete He desorption and to investigate the role of Si crystallization and defect evolution. The relationship with the structural changes occurring in the host coating upon annealing and the effects on the optical properties (refractive index) and bandgap values will be investigated and discussed in the present work.

2. Experimental

To increase the introduction of defects and the disorder in the coating, the deposition conditions were selected to achieve the highest He incorporation. As described in [12] a high He/Si ratio is obtained when Helium working pressures of 2.7 Pa was used [12]. The coatings reported in this work were deposited at 150 W in rf mode using 2.7 Pa of He from a pure silicon target (2″) placed at 5 cm from the sample holder, details on the procedure can be found in [12]. The coatings were prepared on silicon (1 0 0) and fused silica substrates deposited simultaneously. Annealing treatments were performed in He atmosphere (He flow 100 ml/min in a tubular furnace Thermolyne 59300), on samples deposited on Si and fused silica for chemical, microstructural and optical investigations. A 10 °C/min ramp was used until the desired annealing temperature was reached, the samples were then heat treated for 120 min and then cooled to room temperature inside the furnace.

The composition of the coatings was evaluated by nondestructive Ion Beam Analysis (IBA) techniques at the 3 MV NEC 9SDH-2 tandem accelerator of the National Center for Accelerators (CNA, Seville, Spain). Proton elastic backscattering spectrometry (p-EBS) following the method described in [41] using a beam of 2.0 and 1.0 MeV and a Passivated Implanted Planar Silicon (PIPS) detector set at 165°, was used to determine the amounts of He and Si in the coating. The p-EBS spectra were analyzed with SIMNRA software [42] using the evaluated (SigmaCalc) cross-sections obtained from the IBANDL database, IAEA base [43]. Carbon and Oxygen contaminations in the films were evaluated by Nuclear Reaction Analysis (NRA) using the reactions $^{16}O(d, p_1)^{17}O$ and $^{12}C(d,p)^{13}C$ with deuterium ions of 890 and 990 keV.

The thickness and morphology of the samples were examined by scanning electron microscopy (HITACHI S-4800 SEM-FEG). The samples deposited on silicon substrates were cleaved and observed without metallization in cross-sectional views at 1–2 kV.

The microstructure of the annealed coatings was first investigated by X-ray diffraction (XRD) measurements on samples deposited on fused silica substrates. The measurements were performed using Cu Kα radiation in a Siemens D5000 diffractometer in a Bragg-Brentano configuration in the 2θ angle range of 10–90°.

The microstructure of the porous films was also investigated using transmission electron microscopes (TEM) at the Laboratory of Nanoscopies and Spectroscopies (LANE-ICMS, Sevilla, Spain) equipped with a Philips CM200 and a Tecnai G2 F30 operating at 200 and 300 kV respectively. The cross-sectional TEM samples were prepared from the coatings deposited on silicon, by mechanical polishing and dimple grinding, followed by Ar+ ion milling to electron transparency. The pore distribution was evaluated from the TEM micrographs by binarizing them and then using the analyze particles function of ImageJ software32 [43].

The optical characterization of the coatings was performed by ellipsometry on samples deposited on fused silica substrates. The measurements were executed in a UVISEL spectroscopic ellipsometer from HORIBA Jobin Yvon with an incidence angle of 60° and a wavelength range of 300–2100 nm. The data were analyzed using the Deltapsi2 software developed by the HORIBA Jobin Yvon Company.

The optical transmittance of the coatings was measured using a LAMBDA 750S UV/Vis spectrometer in the range 200–2500 nm.

3. Results and discussion

3.1. Morphology and microstructure evolution during annealing

Fig. 1 presents the SEM (a and a.1) and TEM (b and b.1) bright-field cross-sectional views of the as deposited sample. As expected a highly porous coating was grown under the selected deposition conditions. A homogenous pore distribution, all through the coating thickness can be appreciated from the SEM cross sectional views (pores correspond to darker contrasts in SEM images a and a1: as an example, 2 pores are marked in red in a.1). The TEM images reveal in more detail the ellipsoidal pore shape (lighter contrasts in images b and b1, as an example, 2 pores are marked in red in image b1) and also its orientation that depends on the geometry of deposition system and the selected deposition conditions (further information on this can be found in [5,16]). The selected area electron diffraction (SAED) pattern included in Fig. 1b confirms the amorphous structure of the film.

The composition of the coating was checked by p-EBS, the measured and simulated spectra of the as deposited sample are presented in Fig. 2a and b for beams of 2.0 and 1.0 MeV respectively. The results show that the coating is composed mainly by Si and He with a high amount of He incorporated to the coating (~43 at%, check Table 1). The amounts of O and C (as contaminants) in the coatings were further investigated by NRA and the results are presented in Fig. 2c. The simulations reveal small amounts of these elements, lower than 2.0 at%. The composition of the coating is presented in Table 1.

The a-Si:He coatings investigated in the present work were annealed at temperatures of 300 °C, 550 °C, 650 °C and 1200 °C in He atmosphere. It is worth mentioning that all treated samples were deposited simultaneously, either on Si or fused silica substrates, or in different batches using the same deposition conditions and presenting similar composition and microstructure to the formerly presented results. The methodology followed for sample preparation is proved to give reproducible and stable coatings [12].

The coatings' microstructural evolution due to the annealing treatments was first checked by XRD. Fig. 3 presents the diffraction pattern of the as deposited coating compared to the ones of the samples subjected to annealing at 300 °C, 550 °C, 650° and 1200 °C. Up to 550 °C the

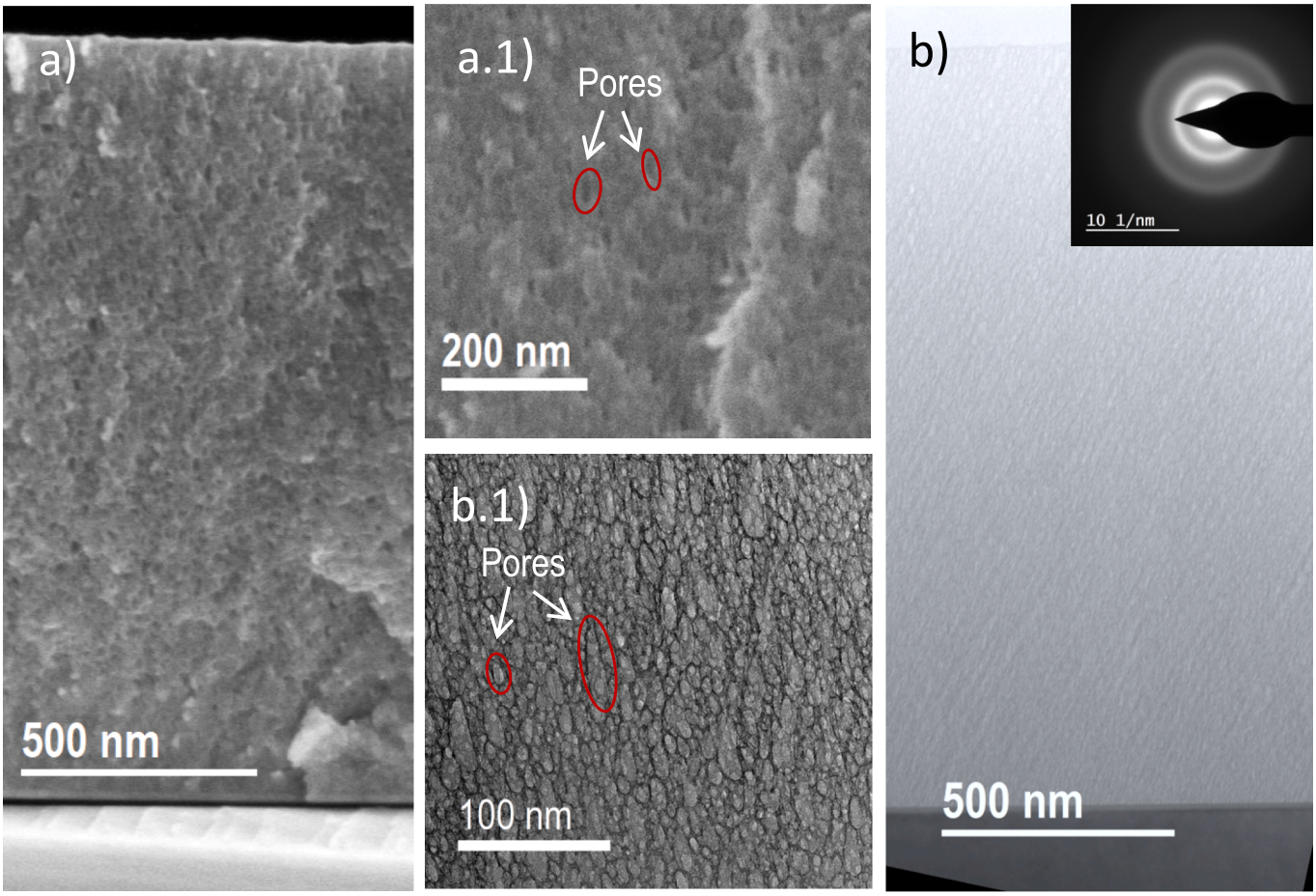

Fig. 1. A) SEM cross-sectional view of the as deposited coating, a1) detail of the pores, b) TEM cross-sectional view with SAED pattern, b1) detail of the pores.

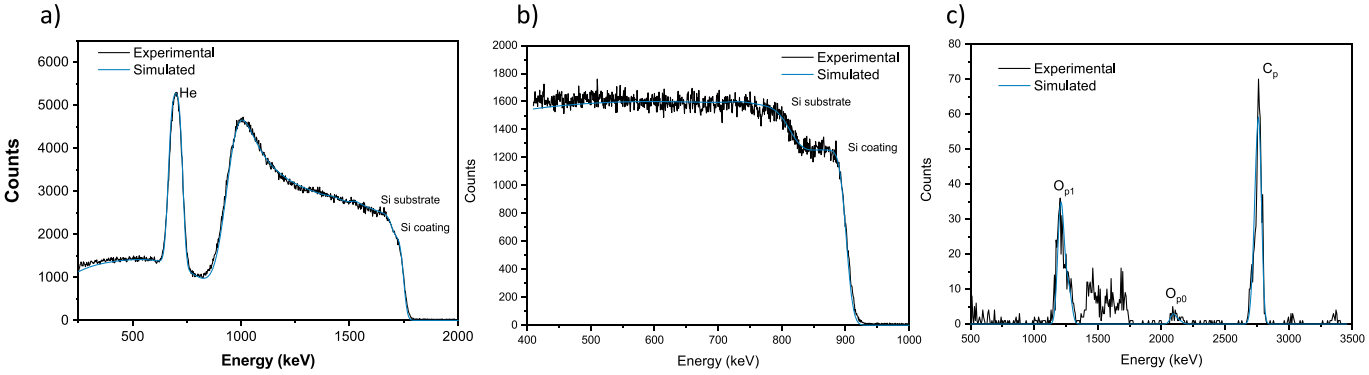

Fig. 2. a) p-EBS spectrum at 2.0 MeV, b) p-EBS spectrum at 1.0 MeV, c) NRA with deuterium ions at 890 keV.

Table 1
Composition as given by p-EBS and NRA.

Sample	Annealing temperature	Si (%at)	He (%at)	O* (%at)	C* (%at)
a-Si:He_as dep	–	54.5 ± 0.9	43.0 ± 1.1	1.7 ± 0.1	0.8 ± 0.1
a-Si:He_300	300	56.5 ± 0.9	41.0 ± 1.1	1.9 ± 0.1	0.6 ± 0.1
a-Si:He_550	550	88.0 ± 0.9	5.0 ± 1.1	5.0 ± 0.1	2.0 ± 0.1
a-Si: He_1200	1200	88.2 ± 0.9	–	9.4 ± 0.1	2.4 ± 0.1

coating remains amorphous. At 650 °C a peak appears around 28.6° corresponding to the (111) plane of Si, that becomes stronger and narrower for the coating annealed at 1200 °C. At 1200 °C also two smaller peaks, at 47.5° and 56.3°, corresponding to (220) and (311) crystallographic planes of Si were observed. Similar results were found in a recent study by "in-situ" XRD analysis under annealing in vacuum [24].

The morphological and microstructural changes upon annealing in Helium flux were also investigated by electron microscopy by both SEM and TEM. Fig. 4 presents micrographs with details of the cross-sections of the heat-treated coatings. Observing the coatings' microstructure by SEM micrographs (Fig. 4 a and b) annealing treatments at 300 °C and up to 550 °C result in no relevant changes when compared to the as

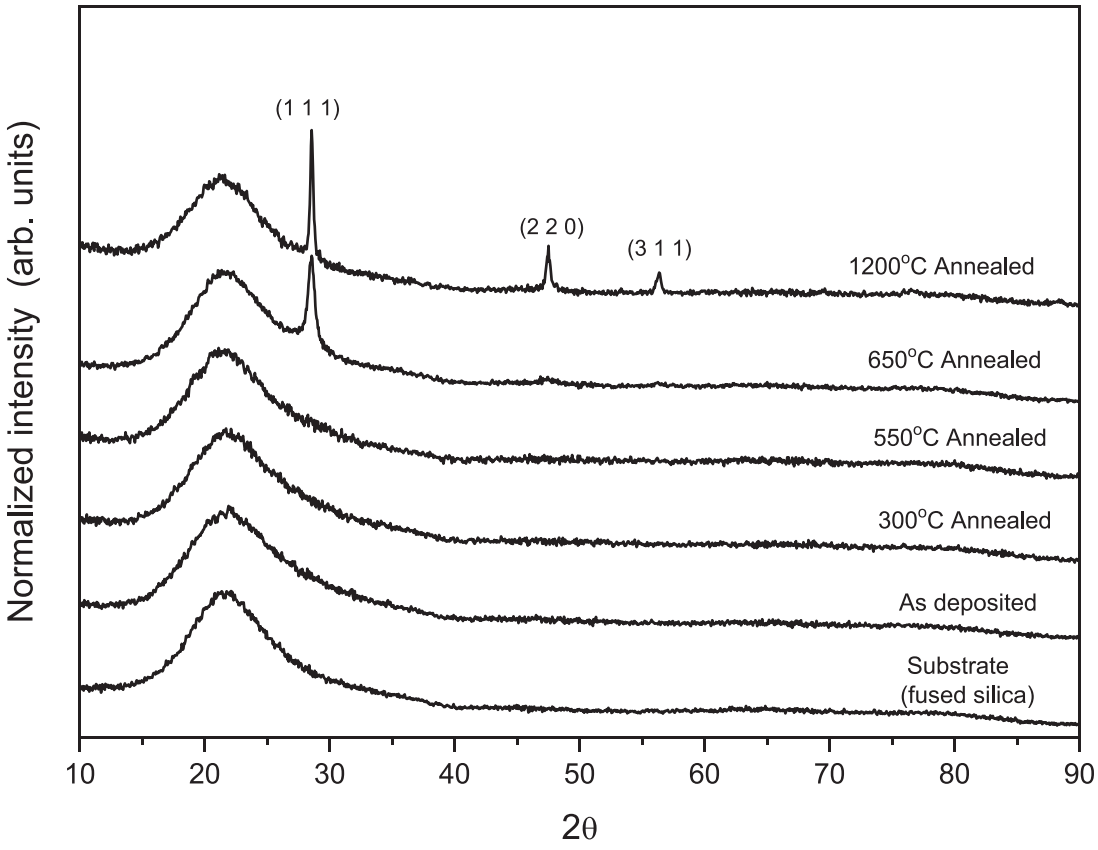

Fig. 3. XRD patterns of the as-deposited a-Si:He coating and after annealing at 300 °C, 550 °C, 650 °C and 1200 °C for samples deposited on fused silica substrates. Peak positions for crystallographic planes of Si are indicated.

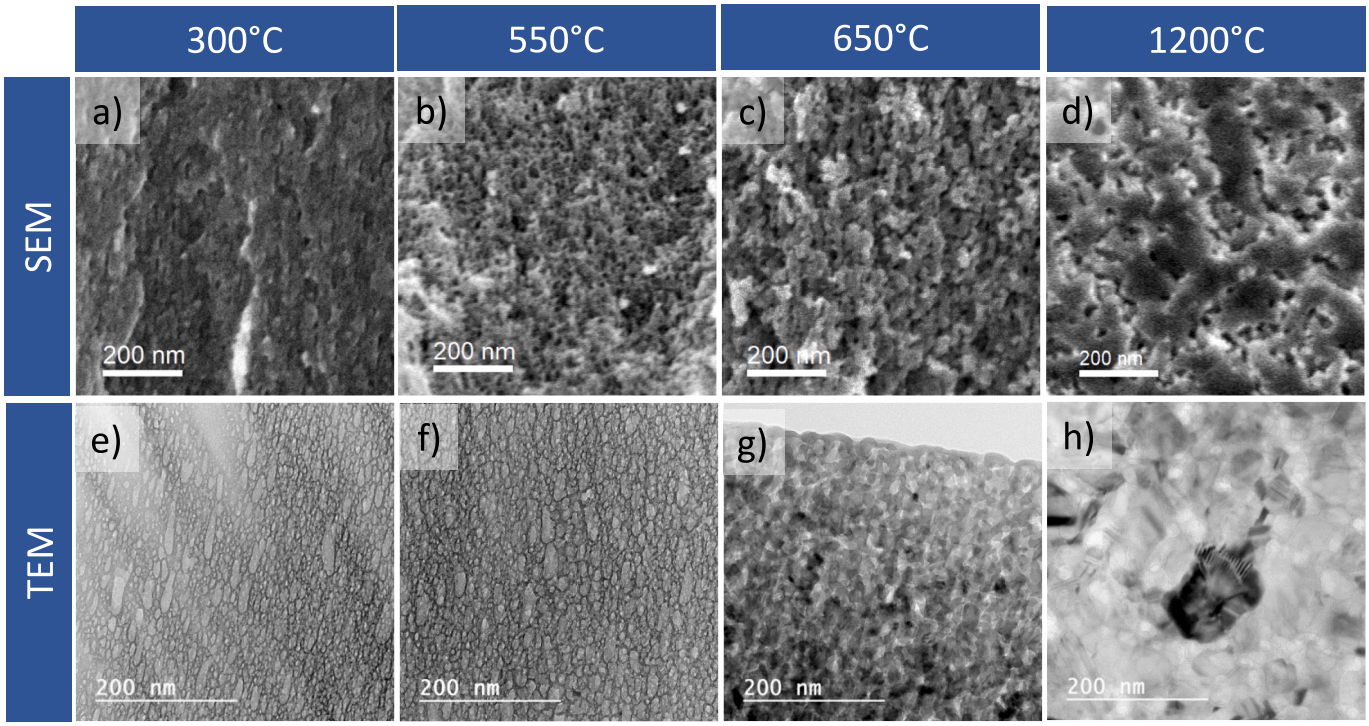

Fig. 4. From a) to d) SEM cross sectional micrographs of samples treated at 300°C, 550°C, 650°C and 1200°C; from e) to h) TEM cross-sections of the coatings annealed at 300°C, 550°C, 650°C and 1200 °C.

deposited sample. However, analyzing the TEM cross-sectional views of these samples some differences in pore size are observed (Fig. 4 e and f). To better appreciate these differences, the major and minor diameters of the ellipsoidal pores were evaluated over 150 pores using the ImageJ software and are presented in Table 2. For both dimensions the minimum and maximum values observed as well as the calculated mean value and the respective standard deviation are presented, comparing the results for as deposited and annealed samples at 300 °C and 550 °C. Although in all samples very small pores are observed (see values of minimum major and minor diameters ≤3.5 nm) a clear increase in pore size is observed from the as-deposited sample (maximum major diameter of ~43 nm) to the one treated at 300 °C (with pore sizes up to 73 nm), which slightly decreases with the increasing of the annealing temperature to 550 °C (~67 nm), while keeping similar values in minor diameter (from 15 to 20 nm).

By increasing the annealing temperature to 650 °C, the SEM image (Fig. 4 c) reveals a microstructure with certain interconnectivity between the different pores that is better observed from the TEM micrograph (Fig. 4 g). The XRD results showed the presence of silicon crystalline phase at this temperature. Ordering of silicon atoms to form crystallites could lead to some contraction favoring the widening and interconnectivity of pores. This effect is more pronounced for the sample annealed at 1200 °C, with the appearance of large Si crystals (Fig. 4 h). A clear pore size analysis of the samples subjected to 650 °C and 1200 °C, for comparison with the previous samples, is rather difficult since pores are interconnected. The SAED patterns presented in Fig. 5 confirm the crystallization of the coatings with diffraction rings for the coating annealed at 650 °C and spots for the sample treated at 1200 °C that correspond to nanocrystalline silicon.

The composition of the annealed samples was followed by p-EBS and NRA and the results are presented in Table 1 and Fig. 6. In Fig. 6 the p-EBS spectra of the as deposited sample is compared to the ones of the annealed coatings. Annealing treatment at 300 °C does not seem to have a strong effect on the composition of the coating; a slight decrease of the He amount is observed (5% He loss). This effect could be associated with a certain loss of He trough effusion. The diffusion of He and aggregation of small pores to form bigger pores was reported to be presented at low temperature and further induced by the vacuum annealing temperature and duration [25] explaining the moderate increase in pore size observed after annealing at 300 °C.

In the case of He implanted samples it is reported that at temperatures higher than 300 °C He permeates from bubbles [25]. An irregular pore shape can be appreciated in some pores in Fig. 4e) as if they were the result of merging of other smaller pores. When increasing the annealing temperature in helium up to 550 °C this effect is also observed and most of the He (88 %) is diffused out of the sample (only 5 at% He remains) leaving a closed porous structure as already reported for annealing in vacuum[24]. Figure S1 in supporting information shows high-resolution TEM cross sectional views comparing in more detail the pore shapes of the as deposited sample and the annealed at 300 °C and 550 °C. At 1200 °C no He signal was detected by p-EBS. Similar results were reported for annealing treatments performed on He implanted silicon [14,25]. Also Liu and co-workers [35] investigated the defect characteristics related to helium and its thermal release behavior from helium-charged titanium coatings deposited by magnetron sputtering. Their work points how He desorption is close related to the trapping state being limited by the energy needed for its dissociation from the trapping sites. They attributed desorption at low temperatures to helium at interstitial and surface sites, at middle temperatures desorption would be due the detrapping of helium inside the bubbles, for different size bubbles different activation energies would be needed and at high temperatures helium would release from small clusters of helium-vacancy complexes[35]. In the case of our coatings, the small decrease in helium content observed for sample annealed at 300 °C could be related to the low-temperature desorption from surface and interstitial sites. Raising the annealing temperature up to 550 °C, 88% of the He in the coating was released, most of it from the overpressurized pores. After annealing at 550 °C 5at% of He is still remaining in the coating and higher energy, higher temperature is needed to completely remove it from the coating. The presence of O and C in the annealed coatings was also followed, and checked by NRA in the case of the samples treated at 1200 °C. An increase of O and C content is observed, most probably associated to the formation of an open structure.

Previous works on He charged metal thin films prepared by magnetron sputtering [27,36] discuss the effects of annealing temperature on He desorption and microstructural evolution from microscopic bubbles to macroscopic effects as blistering and bursting. Wang *et al.* [27] report that blistering is a consequence of He diffusion and concentration at the interface between the films and the substrate. The size (from several micrometers to hundreds of micrometers) and number of the blisters tends to increase with annealing temperature increasing [27]. As the He atoms concentration increases with temperature the pressure inside these very large pores increases and burst occurs. Also He-charged Si films prepared in a DC discharge mode showed increased surface nanostructuration (and broader bubbles size distribution) with a significant blistering upon annealing in vacuum [24]. Blistering and consequent bursting are strongly affecting the surface and optical properties of the coatings. Surface morphology of the annealed coatings was therefore evaluated by SEM. Fig. 7 shows SEM planar views of the heat-treated samples deposited on fused silica substrates, which will be used in the next section to evaluate the optical properties of the coatings. The surface of the as deposited sample and heat-treated (up to 650 °C) samples are similar and smooth. However, blistering occurs in the case of the samples deposited on silicon substrates. Figure S2 shows as an example the surface and cross section of annealed samples on silicon substrates presenting blisters. The composition of the coating deposited on fused silica was checked to discard that compositional changes could be the reason for this effect, Table S1 shows a comparison of compositions obtained by p-EBS for samples deposited on silicon and on fused silica, heat treated at 550 °C. No compositional changes were observed. Further work should be performed to investigate the influence of the substrate in blistering.

3.2. Optical properties of the annealed coatings

First of all, it is relevant to place this work in the context of how the introduction of different amounts of He in the a-Si films alters the refractive index of the coatings. Fig. 8a) compares the refractive index as a function of the wavelength for the as deposited *a-Si:He* coating prepared in this work (with He/Si of 0.78) with a coating presenting lower He content (He/Si of 0.58) and also a dense Si coating fabricated by magnetron sputtering using Ar and substrate bias (details on deposition conditions and characterization of these coatings can be found in [5,12]). As can be appreciated an increase in the He content leads to a

Table 2
Statistics on pore sizes from TEM micrographs (over 150 pores analyzed).

Sample	Annealing temperature	Major diameter (nm)				Minor diameter (nm)			
		Min	Max	Mean	σ*	Min	Max	Mean	σ*
a-Si:He_as dep	–	3.3	43.1	14.3	8.2	1.7	15	6.8	2.5
a-Si:He_300	300	3.4	73.2	23.3	14.7	2.5	18.4	8.5	3.1
a-Si:He_550	550	3.5	67.1	20.5	13.9	1.7	20.4	8.8	3.4

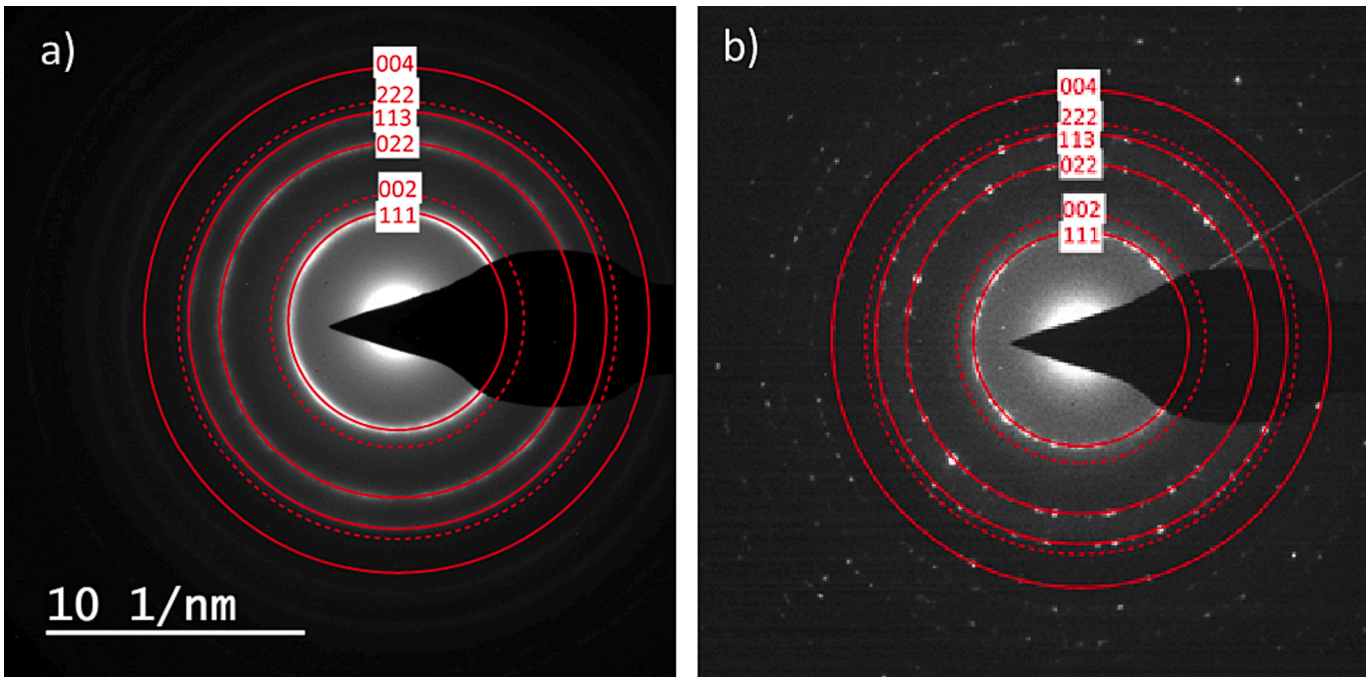

Fig. 5. SAED a) sample annealed at 650°C, b) sample annealed at 1200°C

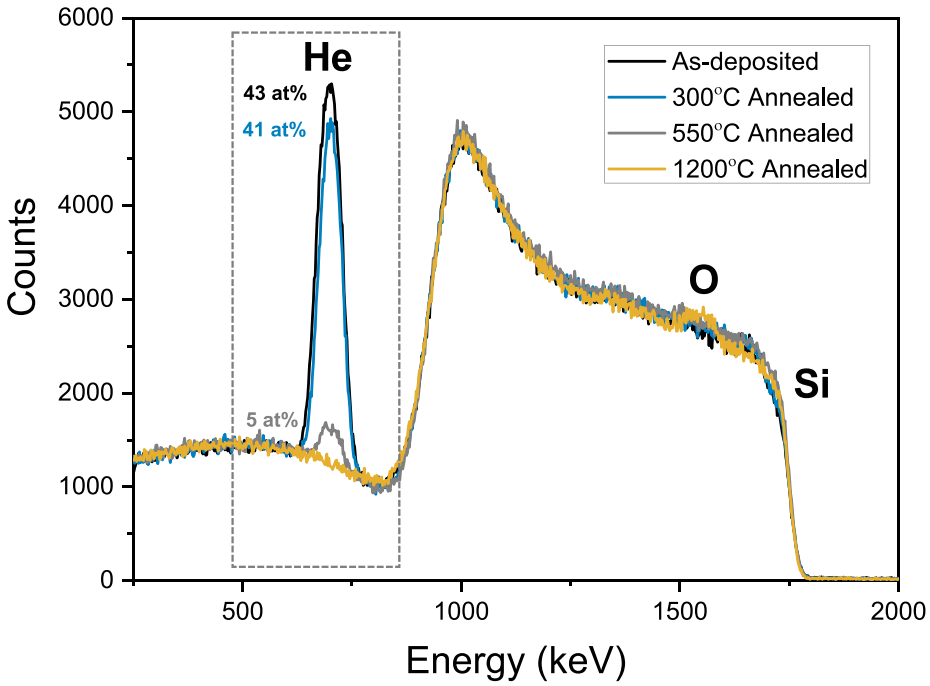

Fig. 6. p-EBS spectra at 2 MeV, comparison of the as deposited coating with samples annealed at 300°C, 550°C and 1200°C

significant decrease of the refractive index (n) of the *a-Si:He* coatings associated to a higher total porosity as compared to the high n presented by the dense coating.

The microstructural and compositional changes during annealing may have also an effect on the optical and electronic properties. Fig. 8b) and c) present the refraction index and extinction coefficient from ellipsometry measurements of the as prepared and annealed samples (up to 650 °C). Experimental and fit data of ellipsometry data are presented in figure S3. A three-layer model (see sketch in Figure S3) composed by the substrate (fused silica), the porous coating and a surface layer was used. To model the porous coating, we have chosen the simplest model, employing an Effective Medium Approximation (Bruggeman) mixture of Tauc-Lorentz oscillator and void. The model fits well the experimental data with Mean Square Error values of 10.4, 9.1 and 6.2 for the as deposit, 550 °C and 650 °C annealed samples respectively. A good agreement was also found between the samples' thickness values obtained by SEM cross-sectional views and those given by ellipsometry, values are presented in Table S2. As it can be appreciated in the selected wavelength range the coatings present similar optical response. Fig. 8b) shows that with increased annealing temperature to 550 °C there is a small increase in the refractive index that can be associated with a certain densification due to the rearrangement of the porous structure

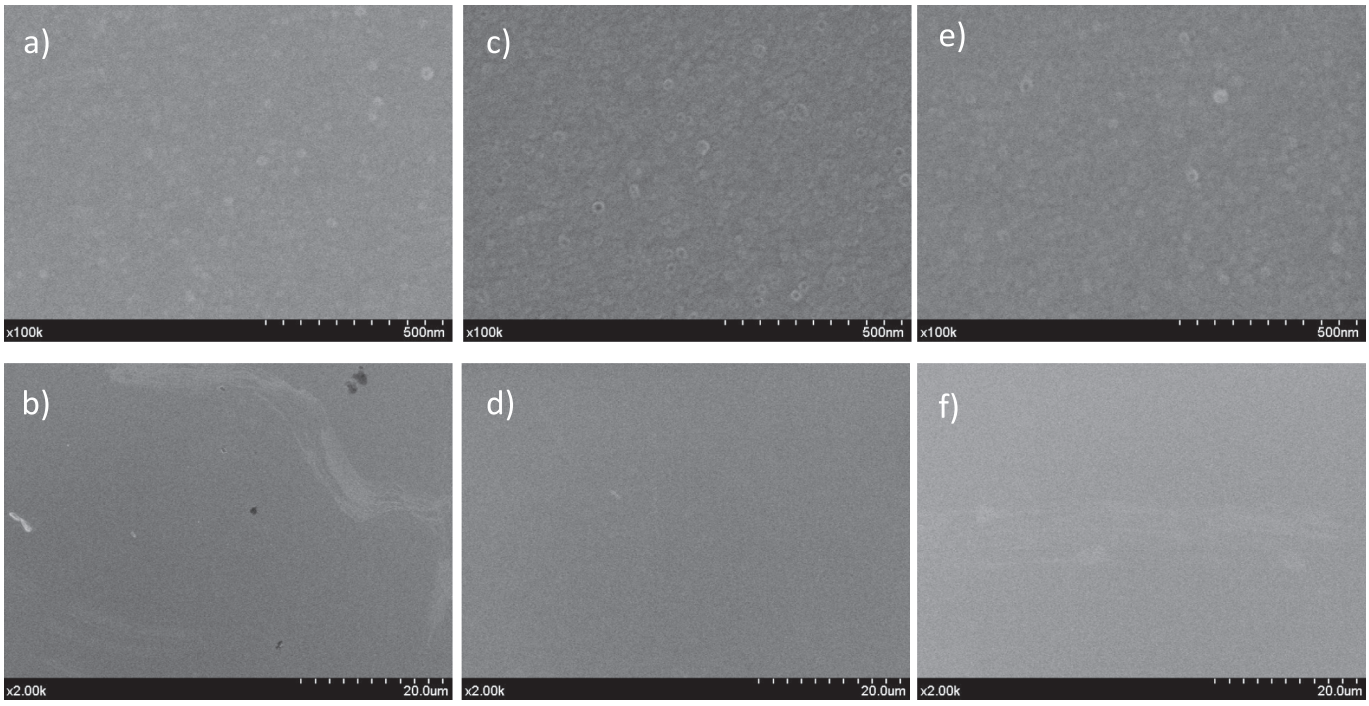

Fig. 7. SEM planar views of samples deposited fused silica. Comparison of as deposited (a and b) and heat-treated surfaces at 550 °C (c and d) and 650 °C (e and f).

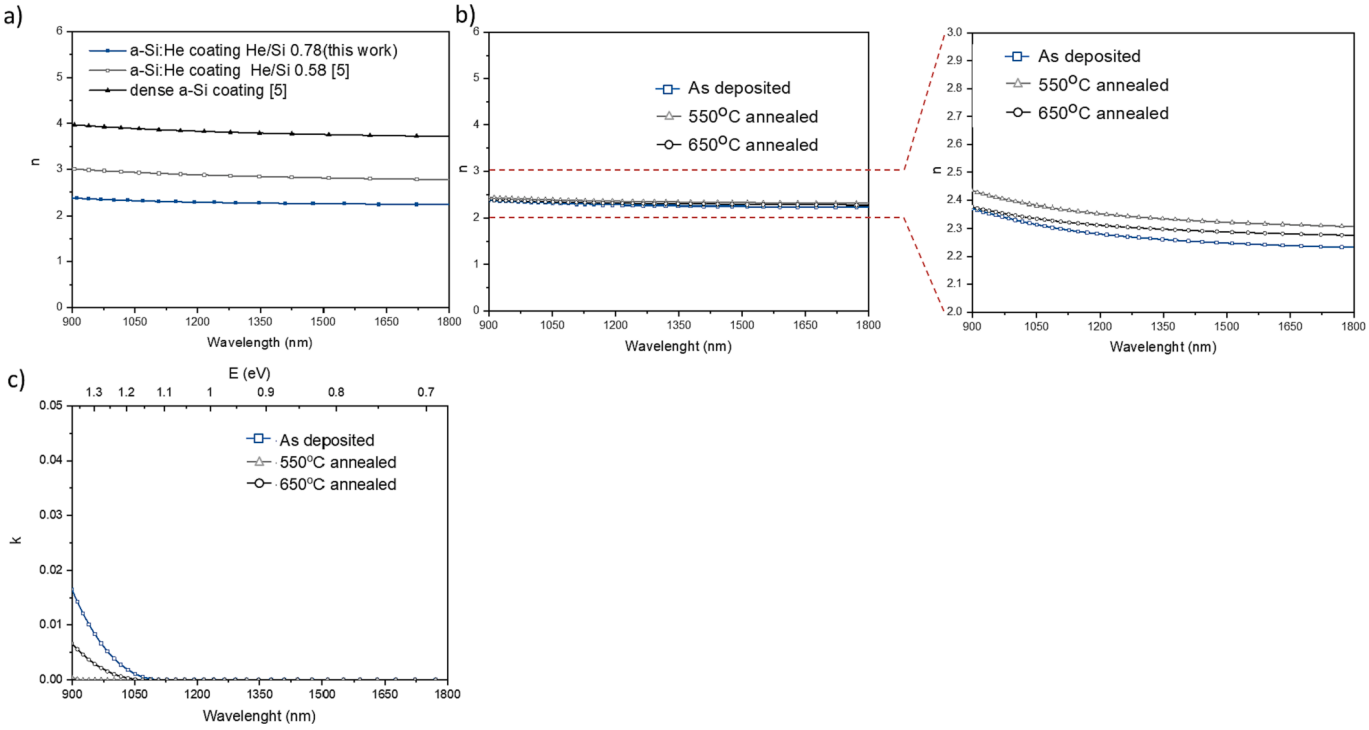

Fig. 8. A) Effect of He incorporation on the refractive index of porous a-Si:He coatings, b) refractive index and c) extinction coefficient of the annealed samples in comparison to the as deposited one.

and He mobility during annealing. Further increasing the annealing temperature to 650 °C lead to the crystallization of silicon passing from a long ranged disordered amorphous porous structure to a nanocrystalline structure where amorphous phase, voids and crystals are present. Moreover, the interconnectivity between pores is pronounced and pores may be open up to the coating surface which can promote pore surface oxidation that can also contribute to reduce the refractive index. Although this effect should be taken into consideration it's worth mentioning that a maximum of 9.4 at% of O was measured from NRA for the samples treated at 1200 °C in helium atmosphere. That would represent the maximum oxidation in the case of this work (see Table 1).

Is worth mentioning that in this work we have not measured the mechanical properties of the coatings, but a certain degree of stress relief during annealing of the overpressurized could be expected, contributing

to the irreversible changes observed in the microstructure of the coatings and affecting the optical properties as previously described by other authors[44].

A reduction of the extinction coefficient (k) is also observed with the increasing of the annealing temperature (Fig. 8c), being close to zero at wavelengths of ~900 nm for the sample annealed at 550 °C, while similar k values are obtained at ~1050 nm for the sample heat treated at 650 °C and 1090 nm for the as deposited sample. These differences can be associated with the previously exposed densification of the a-Si:He_550 sample and densification plus crystallization and possible oxidation of the sample submitted to 650 °C[45].

The changes in structure and ordering due to annealing may affect also the band gap (Eg) of silicon coating. The optical band gap of the a-Si:He samples in the different conditions could present a wide range of variation as the coating structure changes from amorphous silicon with overpressurized He pores, to an amorphous silicon matrix with voids and finally to a more complex nanocomposite structure with amorphous and nanocrystalline phases with voids. We have calculated the Eg from UV–Vis transmission spectra (see figure S4) using Tauc's equation. Fig. 9 presents the results of UV–Vis Tauc's plot for samples as deposited and annealed at 550 and 650 °C.

Most of the works in literature correlate Eg with structure evolution or compositional changes (namely H or O content) of hydrogenated amorphous silicon[46]. Changes in Eg are correlated with the form and content of hydrogen bonding. In our case FTIR measurements were performed to evaluate Si-H and Si-O bonding and to discard their effects on the Eg. Figure S5 presents similar spectra for the as deposited and the annealed samples, suggesting that in our case the variations in Eg must be related with the structural changes. The effects of amorphous phase in optical band gap of silicon and the effects of topological disorder and defects have been previously investigated. The increase of structural disorder reduces de Tauc bandgap of a-Si [40]. In our results we observe lower Eg value for the as deposited a-Si:He sample (Eg = 1.37 eV). This value agrees with previously reported bandgap values for unhydrogenated a-Si [47,48]. As the annealing temperature is increased, ordering of the porous a-Si:He structure takes place while He is released. The a-Si: He_650 coating presenting small crystals of around 13 nm introducing an ordered structure in the amorphous porous matrix presents a Eg of 1.80 eV.

4. Conclusions

In this work we investigated the thermal evolution and properties of amorphous silicon coatings incorporating a high amount of He in overpressurized pores. The coatings were deposited by magnetron sputtering in helium atmosphere followed by annealing treatments also in helium atmosphere from 300 °C up to 1200 °C. The results indicate that the optical and electronic properties of the coatings before and after annealing are closely related to their microstructure. Apart from the reduction in refractive index going from dense to porous He charged Si films, no significant changes in the refractive index of the annealed porous samples are observed. Nevertheless, according to microstructural analysis, at low temperature (300 °C) helium mobility is promoted with merging of pores and a certain densification and rearrangement of the porous structure is observed. This effect is more significant with the increase of annealing temperature up to 550 °C and a small increase in the refractive index is observed. At this temperature a great amount of He is already released from the sample. At 650 °C the sample presents in addition to voids (empty pores) small Si crystals (13 nm). Introducing an ordered structure by annealing leads to significant changes in the bandgap of the coating (from 1.37 eV for the as deposited coating to 1.80 eV for the 650 °C annealed sample). Annealing at high temperatures as 1200 °C leads to a structure of open porosity with bigger crystals.

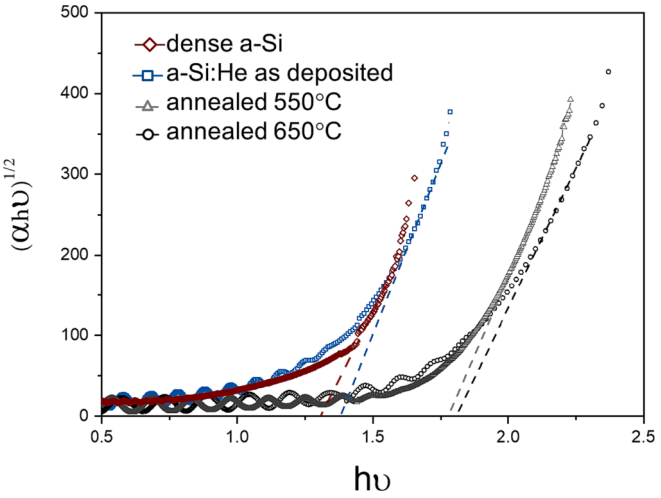

Fig. 9. Tauc's plot.

CRediT authorship contribution statement

V. Godinho: Investigation, Supervision, Conceptualization, Writing – original draft, Writing – review & editing. **J. Caballero-Hernández:** Investigation, Visualization, Methodology. **B. Lacroix:** Investigation, Data curation, Writing – review & editing. **F.J. Ferrer:** Investigation, Data curation, Writing – review & editing. **D. Jamon:** Investigation, Data curation, Writing – review & editing. **M.C. Jiménez de Haro:** Investigation, Data curation, Writing – review & editing. **A. Fernández:** Funding acquisition, Investigation, Supervision, Conceptualization, Writing – review & editing.

Declaration of Competing Interest

The authors declare the following financial interests/personal relationships which may be considered as potential competing interests: Asuncion Fernandez reports financial support was provided by Spanish Ministry of Science and Innovation and Universities. Asuncion Fernandez reports financial support was provided by Junta de Andalucia.

Data availability

Data will be made available on request.

Acknowledgements

This work was supported by the Spanish Ministry of Science and Innovation and Universities under grants nr. PID2021-124439NB-I00 and PID2021-123879OB-C21, the Junta de Andalucía under grant nr. P20-00239. All projects were co-financed by EU FEDER funds. The CSIC is also acknowledged for the grant 202160E029. F.J. Ferrer acknowledges the funding of the University of Seville through the "VI Plan Propio de Investigación y Transferencia de la US" (VI PPIT-US).

Appendix A. Supplementary data

Supplementary data to this article can be found online at https://doi.org/10.1016/j.apsusc.2023.158681.

References

[1] S. Kajita, et al., Enhanced growth of large-scale nanostructures with metallic ion precipitation in helium plasmas, Sci. Rep. 8 (1) (2018).
[2] I. Tanyeli, et al., Nanostructuring of Iron Surfaces by Low-Energy Helium Ions, ACS Appl. Mater. Interfaces 6 (5) (2014) 3462–3468.

[3] S. Iyyakkunnel, et al., Morphological Changes of Tungsten Surfaces by Low-Flux Helium Plasma Treatment and Helium Incorporation via Magnetron Sputtering, ACS Appl. Mater. Interfaces 6 (14) (2014) 11609–11616.

[4] A. Lomov, et al., The microstructure of Si surface layers after plasma-immersion He + ion implantation and subsequent thermal annealing, J. Appl. Crystallogr. 50 (2) (2017) 539–546, https://doi.org/10.1107/S1600576717003259.

[5] V. Godinho, et al., A new bottom-up methodology to produce silicon layers with a closed porosity nanostructure and reduced refractive index, Nanotechnology 24 (27) (2013), 275604.

[6] V. Godinho, et al., On the formation of the porous structure in nanostructured a-Si coatings deposited by dc magnetron sputtering at oblique angles, Nanotechnology 25 (35) (2014), 355705.

[7] R. Schierholz, et al., STEM-EELS analysis reveals stable highdensity He in nanopores of amorphous silicon coatings deposited by magnetron sputtering, Nanotechnology 26 (7) (2015).

[8] T.J. Petty, J.W. Bradley, Tungsten nanostructure formation in a magnetron sputtering device, J. Nucl. Mater. 453 (1) (2014) 320–322.

[9] J. Sakabe, et al., Porous amorphous silicon film anodes for high-capacity and stable all-solid-state lithium batteries, Commun. Chem. 1 (1) (2018) 24.

[10] J.G. Ovejero, et al., Exchange bias and two steps magnetization reversal in porous Co/CoO layer, Mater. Des. 171 (2019), 107691.

[11] W. Fu, et al., Effects of Embedded Helium on the Microstructure and Mechanical Properties of Erbium Films, Nanomaterials 9 (11) (2019).

[12] V. Godinho, et al., Characterization and Validation of a-Si Magnetron-Sputtered Thin Films as Solid He Targets with High Stability for Nuclear Reactions, ACS Omega 1 (6) (2016) 1229–1238.

[13] J. Dérès, et al., Properties of helium bubbles in covalent systems at the nanoscale: A combined numerical and experimental study, Phys. Rev. B 96 (1) (2017), 014110.

[14] K. Alix, et al., Evolution of the properties of helium nanobubbles during in situ annealing probed by spectrum imaging in the transmission electron microscope, Phys. Rev. B 97 (10) (2018), 104102.

[15] V. Raineri, M. Saggio, E. Rimini, Voids in Silicon by He Implantation: From Basic to Applications, J. Mater. Res. 15 (07) (2000) 1449–1477.

[16] J. Caballero-Hernandez, et al., Fabrication of Optical Multilayer Devices from Porous Silicon Coatings with Closed Porosity by Magnetron Sputtering, ACS Appl. Mater. Interfaces 7 (25) (2015) 13889–13897.

[17] F.J. Ferrer, et al., Novel solid ^{4}He targets for experimental studies on nuclear reactions: ^{6}Li + ^{4}He differential cross-section measurement at incident energy of 5.5 MeV, Eur. Phys. J. Plus 135 (6) (2020) 465.

[18] A. Fernández, et al., Low gas consumption fabrication of ^{3}He solid targets for nuclear reactions, Mater. Des. 186 (2020), 108337.

[19] K. Shin, et al., Nanostructured Black Metal: Novel Fabrication Method by Use of Self-Growing Helium Bubbles, Appl. Phys Express 3 (8) (2010), 085204.

[20] M. de Respinis, et al., Efficient Plasma Route to Nanostructure Materials: Case Study on the Use of m-WO3 for Solar Water Splitting, ACS Appl. Mater. Interfaces 5 (15) (2013) 7621–7625.

[21] K. Komori, et al., Sulfur K-edge XANES for methylene blue in photocatalytic reaction over WO_3 nanomaterials, Nucl. Instrum. Methods Phys. Res., Sect. B 365 (2015) 35–38.

[22] S. Kajita, et al., Helium plasma implantation on metals: Nanostructure formation and visible-light photocatalytic response, J. Appl. Phys. 113 (13) (2013), 134301.

[23] B. Lacroix, V. Godinho, A. Fernández, The nanostructure of porous cobalt coatings deposited by magnetron sputtering in helium atmosphere, Micron 108 (2018) 49–54.

[24] A. Fernández, et al., Microstructural characterization and thermal stability of He charged amorphous silicon films prepared by magnetron sputtering in helium, Mater. Chem. Phys. 301 (2023).

[25] V. Raineri, M. Saggio, E. Rimini, Voids in Silicon by He Implantation: From Basic to Applications, J. Mater. Res. 15 (7) (2000) 1449–1477.

[26] L. Pizzagalli, M.L. David, A. Charaf-Eddin, Investigation of helium interstitials aggregation in silicon: Why bubbles formation by a self-trapping mechanism does not work, Nucl. Instrum. Methods Phys. Res., Sect. B 352 (2015) 152–155.

[27] L. Wang, et al., Evolution behavior of helium bubbles and thermal desorption study in helium-charged tungsten film, J. Nucl. Mater. 508 (2018) 107–115.

[28] S. Das, et al., Helium-implantation-induced lattice strains and defects in tungsten probed by X-ray micro-diffraction, Mater. Des. 160 (2018) 1226–1237.

[29] I. Capan, et al., Defects in silicon introduced by helium implantation and subsequent annealing, Radiat. Phys. Chem. 80 (10) (2011) 1099–1103.

[30] V. Raineri, A. Battaglia, E. Rimini, Gettering of metals by He induced voids in silicon, Nucl. Instrum. Methods Phys. Res., Sect. B 96 (1) (1995) 249–252.

[31] M. Bruel, B. Aspar, A.-J. Auberton-Hervé, Smart-Cut: A New Silicon On Insulator Material Technology Based on Hydrogen Implantation and Wafer Bonding, Jpn. J. Appl. Phys. 36 (Part 1, 3B) (1997) 1636–1641, https://doi.org/10.1143/jjap.36.1636.

[32] H. Moriceau, F. Fournel, F. Rieutord, 1 - Materials and manufacturing techniques for silicon-on-insulator (SOI) wafer technology, in: O. Kononchuk, B.-Y. Nguyen (Eds.), Silicon-On-Insulator (SOI) Technology, Woodhead Publishing, 2014, pp. 3-51.

[33] V. Raineri, et al., Radiation damage–He interaction in He implanted Si during bubble formation and their evolution in voids, Nucl. Instrum. Methods Phys. Res., Sect. B 147 (1) (1999) 292–297.

[34] F. Giarratano, et al., Nanoporous Pt-based catalysts prepared by chemical dealloying of magnetron-sputtered Pt-Cu thin films for the catalytic combustion of hydrogen, Appl. Catal. B 235 (2018) 168–176.

[35] C.-Z. Liu, et al., Investigations of helium incorporated into a film deposited by magnetron sputtering, J. Phys. D Appl. Phys. 40 (7) (2007) 2150–2156.

[36] J. Zhang, et al., Thermal evolution of helium in magnetron sputtered titanium films, Nucl. Instrum. Methods Phys. Res. Sect. B: Beam Interactions Mater. Atoms 336 (2014) 6–11.

[37] J. Hartung, J. Weber, Defects created by hydrogen implantation into silicon, Mater. Sci. Eng. B 4 (1) (1989) 47–50.

[38] P.F.P. Fichtner, et al., Overpressurized bubbles versus voids formed in helium implanted and annealed silicon, Appl. Phys. Lett. 70 (6) (1997) 732–734.

[39] V. Raineri, G. Fallica, S. Libertino, Lifetime control in silicon devices by voids induced by He ion implantation, J. Appl. Phys. 79 (12) (1996) 9012–9016.

[40] S. Knief, W. von Niessen, Disorder, defects, and optical absorption in a-Si and a-Si: H, Phys. Rev. B 59 (20) (1999) 12940–12946.

[41] F.J. Ferrer, et al., Simultaneous quantification of light elements in thin films deposited on Si substrates using proton EBS (Elastic Backscattering Spectroscopy), Nucl. Instrum. Methods Phys. Res. Sect. B-Beam Interactions Mater. Atoms 332 (2014) 449–453.

[42] M. Mayer, SIMNRA, a simulation program for the analysis of NRA, RBS and ERDA, AIP Conf. Proc. 475 (1) (1999) 541–544.

[43] C.A. Schneider, W.S. Rasband, K.W. Eliceiri, NIH Image to ImageJ: 25 years of image analysis, Nat. Methods 9 (7) (2012) 671–675.

[44] L. Anghinolfi, et al., Optical properties of uniform, porous, amorphous Ta2O5 coatings on silica: temperature effects, J. Phys. D Appl. Phys. 46 (45) (2013), 455301.

[45] C. Rotaru, S. Nastase, N. Tomozeiu, Amorphous Phase Influence on the Optical Bandgap of Polysilicon. Physica Status Solidi (a), 171(1) (1999) 365-370.

[46] J.D. Escobar-Carrasquilla, et al., Influence of oxygen concentration on the optoelectronic properties of hydrogenated polymorphous silicon thin films, Thin Solid Films 638 (2017) 389–395.

[47] N. Maley, J.S. Lannin, Influence of hydrogen on vibrational and optical properties of a-$Si_{1-x}H_x$ alloys, Phys. Rev. B 36 (2) (1987) 1146–1152.

[48] S.A. Abo-Namous, Y. Zaka, R.W. Fane, Dependence of the Electronic and Optical Properties of Unhydrogenated a-Si on Preparation Conditions, Physica Status Solidi (a), 79(2) (1983) 477-482.